Flow (2021), **1** E1
doi:10.1017/flo.2021.1

FLOW CAMBRIDGE UNIVERSITY PRESS

RESEARCH ARTICLE

Shockwave and rarefaction phenomena in field amplified sample stacking of sample ions

Rajiv Bharadwaj[1] and Juan G. Santiago[2*]

[1]Chemical Engineering Department, Stanford University, Stanford, CA 94305, USA
[2]Mechanical Engineering Department, Stanford University, Stanford, CA 94305, USA
*Corresponding author. E-mail: juan.santiago@stanford.edu

Received: XX 2020; **Revised:** XX XX 2020; **Accepted:** XX XX 2020

Keywords: Electrokinetic systems; Electrophoresis

Abstract

Field amplified sample stacking (FASS) is frequently used to improve detection sensitivity of on-chip electrophoretic assays. FASS involves low conductivity sample buffer and high conductivity running buffer. The typical concentration enhancement is equal to γ, the background-to-sample buffer conductivity ratio. However, deviations from ideal behavior occur frequently in nonlinear regimes of electromigration including asymmetric peak shapes and stacking effects in isoconductive ($\gamma = 1$) buffers. We present an analytical model for the case where the sample concentration is on the order of background ion concentrations. We also present on-chip FASS experiments to describe temporal and spatial evolution of zone boundaries in isoconductive buffer system as well as heterogeneous conductivity buffer systems. The model predicts two regimes of concentration enhancement. The first regime is characterized by a rarefaction wave for sample ion distribution with a final concentration enhancement greater than γ. In the second regime, the sample ion concentration wave steepens toward a shock wave, and maximum concentration enhancement is less than γ. We used epifluorescence imaging in a staggered-T glass microchip (under suppressed electroosmotic flow conditions) to quantify the dynamics of electromigration shock and rarefaction waves in microchannels. There is good quantitative agreement between the predicted and measured maximum concentration enhancement.

Impact Statement

Electrokinetic microfluidic systems have been leveraged for a wide variety of applications including sample preparation, species separation, and detection of chemical and biochemical species. One key functional aspect of such devices is field amplified sample stacking (FASS) which is used to preconcentrate species to improve the limits of detection. We demonstrate how electrophoretically transported species can exhibit shockwave and rarefaction wave phenomena. These result from a non-linear coupling between non-uniform concentration gradients and the direction of ion migration. In particular, we find ionic migration in the direction of decreasing species velocity results in self-steepening of ion gradients into a shock wave. These waves have application to efficient preconcentration of species to improve limit of detection and to species transport with minimal dispersion. Conversely, ion migration in the direction of increasing species velocity results in rarefaction waves. Importantly, experimental observations of such rarefaction waves appear qualitatively as a rapid diffusion, but in fact the dispersion rate of these waves is dominated by the non-uniform species velocity. The analyses identify key controlling parameters governing the dynamics of these waves and offers a method to enhance and suppress them.

1. Introduction

Sample stacking techniques enable high sensitivity microchip-based electrophoretic assays. Several electrokinetic stacking techniques, including field amplified sample stacking (FASS), isotachophoresis (ITP), micellar electrokinetic chromatography (MEKC), iso-electric focusing (IEF), and temperature gradient focusing (TGF), have been successfully applied to microchip-based systems. The sensitivity increase can be anywhere between 10-fold to a millionfold (Jacobson & Ramsey, 1995, Jung, Bharadwaj, & Santiago, 2006a; Jung, Bharadwaj, & Santiago, 2006b). Comprehensive understanding of the physics of stacking processes is critical for optimization of sensitivity of lab-on-a-chip devices.

One of the simplest sample stacking techniques is field amplified sample stacking (FASS). 1000-fold signal increase is possible with this method (Jung, Bharadwaj, & Santiago, 2003; Kuban, Berg, Garcia, & Karlberg, 2001). In FASS, an axial gradient in ionic conductivity (and electric field gradient) is achieved by preparing the sample in an electrolyte solution of lower concentration than the background electrolyte (BGE). Upon application of an axial potential difference, the sample region acts as a high electrical resistance zone in series with the rest of the channel, resulting in a large local electric field within the sample zone. Under the influence of electric field, sample ions migrate from the high to low drift velocity region. This leads to a local accumulation or "stacking" of sample ions near the conductivity interface. This stacking increases sample concentration and results in increased signal. The maximum concentration increase in FASS is proportional to γ, the BGE-to-sample electrolyte conductivity ratio (Bharadwaj, Santiago, & Mohammadi, 2005; Burgi & Chien 1991).

However, deviations from this ideal case are possible under various situations. For example, Burgi and Chien (1991) point out that for sample concentrations greater than 10 μM, conductivity gradients and pH fields can change during FASS injection, resulting in complex behavior not captured by idealized FASS models. Another example of non-ideal FASS was recently provided by Liu, Foote, Jacobson, and Ramsey (2005) they described sample stacking in a MEKC system involving sodium dodecyl sulfate (SDS) micelles. The buffer system in their experiments is characterized by initially isoconductive sample and running buffer. Conventional FASS theory is unable to explain any concentration change in isoconductive buffer system since, $\gamma = 1$. Liu et al. qualitatively argued that the stacking process in isoconductive system is due to mismatch of various ionic transport numbers (although the detailed dynamics of the process were not described).

Several CE researchers have developed fairly comprehensive mathematical models to investigate multi-ion electromigration phenomena such as isotachophoresis and isoelectric focusing (Bier, Palusinski, Mosher, & Saville, 1983; Ermakov, Zhukov, Capelli, & Righetti, 1994; Gas & Kenndler, 2000; Gebaur & Bocek, 1997; Mosher, Saville, & Thormann, 1992). For example, Hruska, Jaros, and Gas (2006) have developed freeware software, Simul 5, that can be used to simulate various linear and non-linear electromigrational systems. Such simulations are extremely useful in designing and optimizing complex non-linear electrokinetic assays. However, derivation of key non-dimensional parameters and detailed evaluation of salient physics can be difficult starting from such large models. The focus of the current paper is to present a simple analytical model that sheds light on various complex non-linear electromigration phenomena in the context of FASS. In particular, we are interested in obtaining key dimensionless parameters governing stacking dynamics, and exploring the generation of ion concentration shock waves and rarefaction waves in the regime where sample concentration is on the order of that of the BGE. In FASS, the concentration scales can easily vary by three orders of magnitude between the high conductivity running buffer and the sample buffer, which is often prepared in DI water. Therefore, the appropriate scaling of parameters is not easily apparent. We have developed a fairly general analytical model for three-ion systems that serves to describe stacking processes in isoconductive and heterogeneous conductivity system. The model shows that the stacking effect is governed by three dimensionless ratios—conductivity ratio (γ), ratio of the sample ion concentration to the counterion concentration (ε), and the ratio of the product of mobility and valence number of sample and co-ions (β). We have performed microchip-based electrophoresis experiments to validate the model. A staggered-T channel microchip was used to generate well-defined interface between heterogeneous electrolyte solutions. We

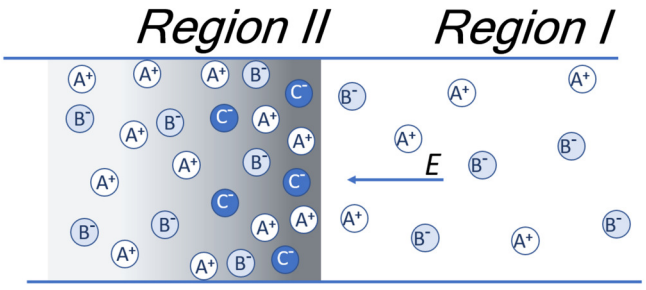

Figure 1. *(a) FASS system with a single sample/BGE interface. Roman numerals I and II denote high conductivity BGE and low conductivity sample regions, respectively.*

used quantitative full-field epifluorescence microscopy to measure the electric field driven temporal and spatial evolution of sample ions. There is good quantitative agreement between the model and experiments. The experimentally validated model can be used to judiciously choose system parameters to control and optimize concentration enhancement and the peak shapes.

2. Theory

We consider one-dimensional electromigration of three, fully ionized ions: A (counter-ion), B (co-ion) and C (sample ion). A constant current density, j_o, is applied in the axial direction and the electrolyte system is assumed to be electrically neutral. The electrophoretic mobility, ν, of various ions is assumed constant. We focus on FASS across single and double electrolyte-electrolyte interfaces as depicted in Figure 1. The single interface configuration describes so-called field amplified sample injection (FASI) (Burgi & Chien, 1991) or large volume sample stacking (LVSS) (Chien, 1992) processes. The system is assumed to have zero electroosmotic flow and we consider the limit of large electromigration-to-diffusive flux ratio (i.e., we neglect diffusion). In real systems, diffusion and convective contribute to dispersion and slow the FASS process (Bharadwaj & Santiago, 2005).

Under these assumptions the governing equations are in dimensionless form:

$$E'(x,t) = \frac{1}{\sigma'(x,t)} \tag{1}$$

$$\frac{\partial C'_A}{\partial t'} = -z_A \frac{\partial}{\partial x}\left(\frac{C'_A}{\sigma'}\right) \tag{2}$$

$$\frac{\partial C'_C}{\partial t'} = -z_C \nu_C \frac{\partial}{\partial x}\left(\frac{C'_C}{\sigma'}\right) \tag{3}$$

Equations (1) is the condition of current conservation, and equations (2) and (3) are the species conservation equation. The concentration of the third ion is determined by the electroneutrality condition:

$$C'_B = -\frac{\left(z_C C'_C + z_A C'_A\right)}{z_B} \tag{4}$$

The dimensionless variables are the following:

$$x' = \frac{x}{s};\ \nu' = \frac{\nu}{\nu_A};\ C' = \frac{C}{C_{Ao}};\ \sigma' = \frac{\sigma}{F^2 \nu_A C_{Ao}};\ t' = \frac{t j_o}{F s C_{Ao}} \tag{5}$$

where $\sigma(x,t) = F^2 \sum z_i^2 \nu_i C_i$ is the electrical conductivity distribution, s is the characteristic length scale of the initial concentration gradients, and C_{Ao}, is the initial counter-ion concentration in the sample region.

The boundary and initial conditions for the concentration fields are for the single electrolyte-electrolyte interface are

$$\begin{aligned} C'_A(x' = -L', t') = \alpha;\ C'_A(x = L', t') = 1;\ \alpha > 1 \\ C'_C(x' = -L', t') = 0;\ C'_C(x = L', t') = \varepsilon. \end{aligned} \tag{6}$$

For a channel length, L, much larger than the characteristic interface length, s, we assume the following initial conditions ion distributions:

$$\begin{aligned} C'_A(x', t' = 0) = 0.5((1+\alpha) + (1-\alpha) erf(x')) \\ C'_C(x', t' = 0) = 0.5\varepsilon(1 + erf(x')) \end{aligned} \tag{7}$$

Here, $\varepsilon = C_{Co}/C_{Ao}$, is the ratio of the initial sample concentration and counter-ion concentration in the sample region. We will drop the primes in the rest of the paper for clarity of presentation.

Further simplification is possible by multiplying equation (2) by $z_A - z_B\nu_B$ and equation (3) $z_C - z_B\nu_B/\nu_C$ and adding the resulting equations; this leads to

$$C_A(x,t)(z_A - z_B\nu_B) + C_C(x,t)(z_C - z_B\nu_B/\nu_C) = f(x) \tag{8}$$

$f(x)$ is determined solely from the initial conditions and can be interpreted as a Kohlrausch regulating function (KRF) (Kohlrausch, 1897). This equation can be solved for C_A in terms of C_C and substituted back in equation (3) to obtain:

$$\frac{\partial C_C}{\partial t} = -z_C \nu_C \frac{\partial}{\partial x}\left(\frac{C_C(x,t)}{\sigma'(C_C)}\right) \tag{9}$$

$$\sigma'(C_C) = z_A f(x) + C_C(x,t)\lambda(\beta - 1) \tag{10}$$

where $\lambda = z_B\nu_B(z_C - z_A/\nu_C)$ and $\beta = z_C\nu_C/z_B\nu_B$. This form of the equations decouples the dynamics of individual ions. We first solve for the C_C from equation (9), and then equations (8), (4), and (1) can be used to obtain C_A, C_B, and the electric field.

The sample ion concentration distribution is governed by a nonlinear hyperbolic equation, and so sharpening (shock waves) or dispersion (rarefaction waves) of concentration can be expected. equations (9) can be written as

$$\frac{\partial C_C}{\partial t} = -\frac{z_C\nu_C f(x)}{\sigma'^2}\frac{\partial C_C}{\partial x} + \frac{z_C z_A \nu_C}{\sigma'^2}\frac{\partial f}{\partial x}C_C. \tag{11}$$

The first term on the right hand side is similar in form to an advection of C_C. The second term is analogous to a rate of generation of ion C. The nondimensional wave velocity is $z_C\nu_C f(x)/\sigma'^2$, where σ' is a function of sample ion concentration C_C. Equation (10) shows that since $\lambda > 1$, wave velocity increases with C_C for $\beta < 1$ and decreases for $\beta > 1$. For $\beta = 1$ the nonlinearity disappears. Later, we will show that β also governs maximum concentration enhancement.

3. Method of Solution

We first note that the nonlinear hyperbolic equation governing sample ion distribution (equation (9)) can be solved using the method of characteristics (MOC). (Bharadwaj & Santiago, 2005; Whitham, 1974). However, the limitation of this MOC solution is that it results in unphysical, multi-valued concentration fields for cases where concentration shock waves form. We therefore use finite volume methods in this paper to solve the nonlinear hyperbolic equation governing sample ion distribution. Finite volume

methods based on the integral form of conservation laws are useful to accurately capture the so-called *weak solutions* involving shock waves. We use the first-order, upwind Godunov's method (Leveque, 2002). to solve equation (9) for the sample ion concentration field, C_C. The time step and the spatial step size were chosen based on the CFL condition. Also, the numerical solutions for the rarefaction regime were verified (results not shown) against analytical solutions obtained using the above-mentioned method of characteristics solution.

4. Kohlrausch Regulating Function (KRF) Analysis

In this section, we consider a special case of FASS in which a sample co-ion is absent in the sample solution. For this special case, the sample region contains only A and C ions, and that the ions of the BGE are A and B. The electroneutrality assumption then requires that $\varepsilon = \varepsilon_{\max} = z_A/|z_C|$, and we can derive a closed-form expression for maximum concentration enhancement using KRF analysis.

Using the initial conditions, given by equation (7), the magnitude of KRF for the sample and BGE regions can be derived as:

$$KRF_S = \frac{C_{Ao}}{\nu_A} - \frac{z_A C_{Ao}}{z_C \nu_C};\ KRF_{BGE} = \frac{\alpha C_{Ao}}{\nu_A} - \frac{z_A \alpha C_{Ao}}{z_C \nu_C} \tag{12}$$

As sample ions exit the initial sample region and enter the BGE region, C_C must conform to KRF_{BGE}. (Foret & Bocek, 1993). This constraint leads to

$$\frac{C_{A,new}}{C_{Ao}} = \frac{C_{C,stack}}{C_{Co}} = \alpha \frac{z_A \nu_A - z_B \nu_B}{z_A \nu_A - z_C \nu_C} \left(\frac{z_C \nu_C}{z_B \nu_B} \right) \tag{13}$$

where, $C_{A,new}$, is the KRF-adjusted concentration of counter-ion. Equation (13) can be expressed in terms of γ, the ratio of sample and BGE conductivity as follows:

$$\gamma = \frac{\sigma_{BGE}}{\sigma_S} = \alpha \frac{z_A \nu_A - z_B \nu_B}{z_A \nu_A - z_C \nu_C} \tag{14}$$

Substituting equation (14) into (13) we obtain:

$$\frac{C_{C,stack}}{C_{Co}} = \gamma \left(\frac{z_C \nu_C}{z_B \nu_B} \right) = \beta \gamma \tag{15}$$

This special case clearly shows that the maximum concentration enhancement can be higher or lower than γ, depending on the magnitude of β.

Next, we shall use solutions of Equation (9) to show that concentration enhancement higher or lower than γ is also possible in the more general case of a system with A, B, and C ions in the sample region and A and B ions in the BGE region.

5. Theoretical Results

The electromigration model developed sheds light on various regimes of FASS dynamics. Figure 2a(i-iii) shows the development of sample ion concentration field, C_C, the BGE ion concentrations, C_A and C_B, and electric field distribution for $\varepsilon \ll 1$. This situation, frequent in practice, is where a sample ion concentration, C_C, is much smaller than that of the BGE. Here, sample ions have a negligible effect on the conductivity field and the electrolyte system behaves as a binary electrolyte composed of A and B ions. Absent diffusion and convection, the concentration distribution is described by the initial condition at all times.[18] This condition has been referred to as the formation of the stationary boundary and is discussed in detail by Bharadwaj and Santiago (2005). Sample ions act as a passive scalar whose electromigration is determined by the electric field distribution established by underlying BGE ions.

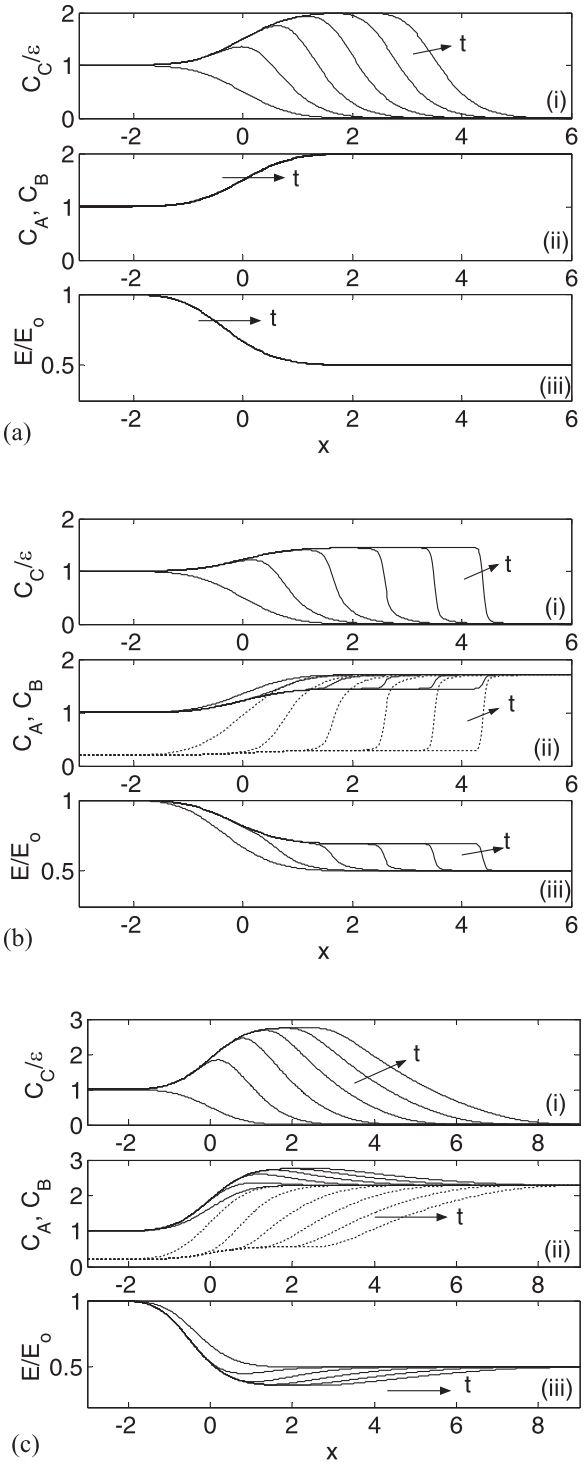

Figure 2. *Spatial and temporal distribution of (i) sample ions, (ii) BGE ions, (iii) electric field for the following three cases: (a) $\gamma = 2$, $\varepsilon = 0.001$, and $\beta = 2/3$; (b) $\gamma = 2$, $\varepsilon = 0.4$, and $\beta = 2/3$; (c) $\gamma = 2$, $\varepsilon = 0.4$, and $\beta = 3/2$. The co-ion distribution, C_B, is represented by dashed lines. The ion valence numbers and mobilities values in all three cases are: $z_A = 1$, $z_B = -1$, $z_C = -2$, $\nu_A = 1$, and $\nu_C = 2$. $\nu_B = 6$ for $\beta = 2/3$ and $\nu_B = 8/3$ for $\beta = 3/2$.*

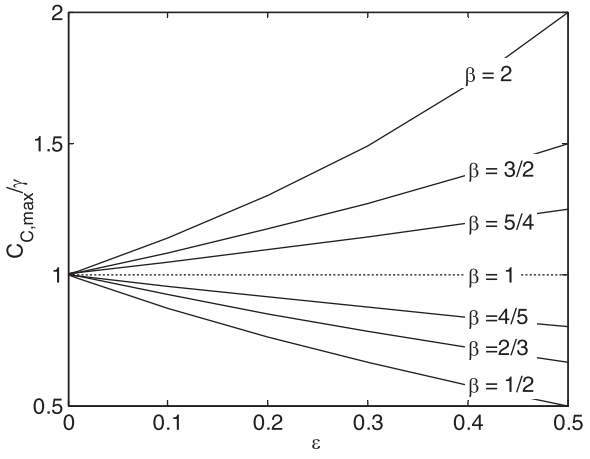

Figure 3. *Summary of three regimes for FASS. Normalized maximum concentration enhancement is plotted as a function of ε and β. The ion valence numbers and mobilities values in all cases are: $z_A = 1$, $z_B = -1$, $z_C = -2$, $\nu_A = 1$, and $\nu_C = 2$. Mobility of the co-ion, ν_B, is fixed by the β value.*

In figures 2b and 2c we study two cases where the sample ion concentration in the initial sample region is comparable to that of BGE ions, so that ε is order unity. This condition arises when the sample is prepared in very low conductivity buffer or DI water, and is also frequent in practice. Figures 2b(i-iii) show results for the case where the sample-ion-to-co-ion ratio of the product of electrophoretic mobility and valence number is less than unity, $\beta < 1$. Figure 2b(i) shows that the maximum concentration enhancement in this regime is lower than γ. Since $\beta < 1$, the sample ion wave velocity increases with sample concentration. This results in a steepening of the concentration profile as the sample stacks, resulting in sharp gradients, and tending toward a concentration shock wave. Figure 2b(ii) shows the concentration distribution of BGE ions, C_A and C_B. The BGE co-ion (C_B) and counter-ion (C_A) do not follow binary electrolyte dynamics but show complex migration behavior. The electric field shows a "two-step" profile with two inflection points. Therefore, the $\beta < 1$ regime is an example of the so-called stable moving boundary electrophoresis (Foret & Bocek, 1993) where the sample ions displace the BGE co-ions locally, Figure 2c describes the case of $\beta > 1$. For this case, sample ion wave velocity decreases with increasing sample concentration, and so concentration shocks cannot form. This rarefaction condition,[21] however, results in a maximum sample ion concentration enhancement greater than γ. Further, the left edge of the concentration profiles becomes progressively "diffuse," despite the absence of diffusion (or any type of dispersion) in the model.

The cases discussed in figures 2b and 2c are fundamentally different than the ideal FASS dynamics of figure 2a. In the latter two cases, sample ions have a strong and dynamic effect on BGE concentration profiles. The concentration enhancement is no longer just a function of the initial conductivity ratio but is sensitive to the electrophoretic mobility of all the ions in the system. In figure 3, we summarize the three regimes of interest. The plot shows the maximum concentration enhancement, $C_{C.max}/C_{Co}$, normalized by conductivity ratio, γ, as a function of ε and for various values of β. This normalization of concentration enhancement is equal to unity for the ideal condition of vanishing ε. For finite ε (i.e., sample ion concentrations on the order of the those of the BGE), the maximum concentration enhancement can be higher than gamma ($\beta > 1$) or lower than gamma ($\beta < 1$). When $\varepsilon = \varepsilon_{max}$ (the special case of only A and C ions in the initial sample region), the concentration enhancement is given by equation (15). The parameter ε governs the transition from the ideal "stationary boundary" FASS regime to a "moving boundary" regime. Figure 3 clearly shows that our model is able to predict stacking effects for iso-conductive buffer systems ($\gamma = 1$) as observed experimentally by Liu et al. (2005).

It is worthwhile to emphasize the similarities and difference between the finite-ε regimes of FASS and isotachophoresis. Similar to ITP, the $\beta < 1$ regime discussed above, is characterized by a self-sharpening effect. In both cases the maximum concentration enhancement is a function of sample ion mobility. In FASS, however, there is only one co-ion so that self-sharpening of the sample occurs only at one boundary between two zones of different conductivity. In ITP, the mobilities of two co-ions bound that of the sample ion and hence lead to self-sharpening effect at both boundaries of the sample zone.

6. Experimental Results and Model Validation

An inverted epifluorescence microscope (Olympus IX70) equipped with a 10X objective (Olympus, NA = 0.4) and a 0.5X demagnifying lens was used for imaging the concentration fields of bodipy dye solutions. Illumination from a mercury lamp was spectrally filtered at the peak absorption and emission wavelengths of 485 nm and 535 nm, respectively. Images were captured using a cooled CCD camera (Cool-SNAP fx, Roper Scientific, Inc., Trenton, NJ) having a 1300×1030 array of square pixels, with 12-bit intensity resolution. A function generator (Agilent, 33120a) was used to externally trigger the CCD camera to acquire images at 30 fps. The exposure time was set to 10 ms. A Borofloat glass microchip (Micralyne, Alberta, Canada) with staggered-T channel geometry was used for all experiments. The width and centerline depth of the microchannel are 50 μm and 20 μm, respectively, and the channels have the characteristic shape of an isotropic wet etch. The lengths of the vertical and horizontal channels are 8 and 85 mm, respectively. The length of the chip's injection region (the center-to-center distance between the two staggered T sections) is 100 μm. A 6 kV voltage supply system (Micralyne, Alberta, Canada) was used to control platinum electrode potentials mated to the chip reservoirs.

The $\beta < 1$ regime can be realized experimentally by using chloride ions as the co-ions, C_B. Chloride ions have a high electrophoretic mobility of 7.9e-8 m^2V/s (Foret & Bocek, 1993). The sample ion was negatively charged bodipy dye ($z_C = -1$, ν_C = 2e-8 m^2V/s, Invitrogen, California) (Bharadwaj et al., 2002). The BGE was prepared by adding NaCl salt to deionized ultra-filtered (DIUF) water (Fisher Scientific, Baltimore, MD). An equal ratio of bodipy dye and sodium hydroxide was added to DIUF water to prepare the sample solution. The dye concentration was 198 μM in all cases. Experiments were performed for three conductivity ratios: γ = 5, 8.5, and 10. For the rarefaction regime ($\beta > 1$), we used HEPES as the co-ion and Alex Fluor 488 (Invitrogen) dye as the sample ions. This combination of ions provides $\beta \sim 2$. The conductivity ratio for this regime was γ = 1.9. The microchip was flushed with acidified poly (ethylene oxide) solution to suppress electroosmotic flow (EOF) using the method described by Preisler and Yeung (1996). Electrical conductivity was measured using a conductivity meter (Pinnacle 542, Corning Inc., New York).

The interface between high and low conductivity electrolyte solutions was generated by applying a vacuum at the north reservoir of the microchip as shown in Figure 4a. Once the interface was established, the vacuum was released and an axial electric field was applied in the right-to-left direction. This initiates stacking of sample ions at the conductivity interface. Figure 4b shows images of the stacking process at selected times. The images show an increase in fluorescence intensity near the interface due to local accumulation of sample ions. The sample ion concentration gradients gradually become sharp and tends toward a sharp shock wave in concentration as predicted by the model for this $\beta < 1$ case. The imaged concentration gradient in the shock region has an axial length scale, w, of about 9 μm. This width was estimated by fitting the concentration profile with an error function of the form, $A(1 - erf(x/w))$, where A is a constant (regression coefficient of R^2 = 0.99). However, this measured 9 μm interface width is largely a function of fluorescence from out-of-focus dye regions, light scatter from channel walls, and other sources of image noise. For example, the measured of the "sharp" liquid-to-substrate interface (at the channel wall) was approximately 7 μm.

For quantitative analysis of the CCD images, a background image is subtracted from the raw image and this difference is normalized by the difference between a flatfield and the background image (Bharadwaj et al., 2006). To compare the two dimensional image data with the one-dimensional model,

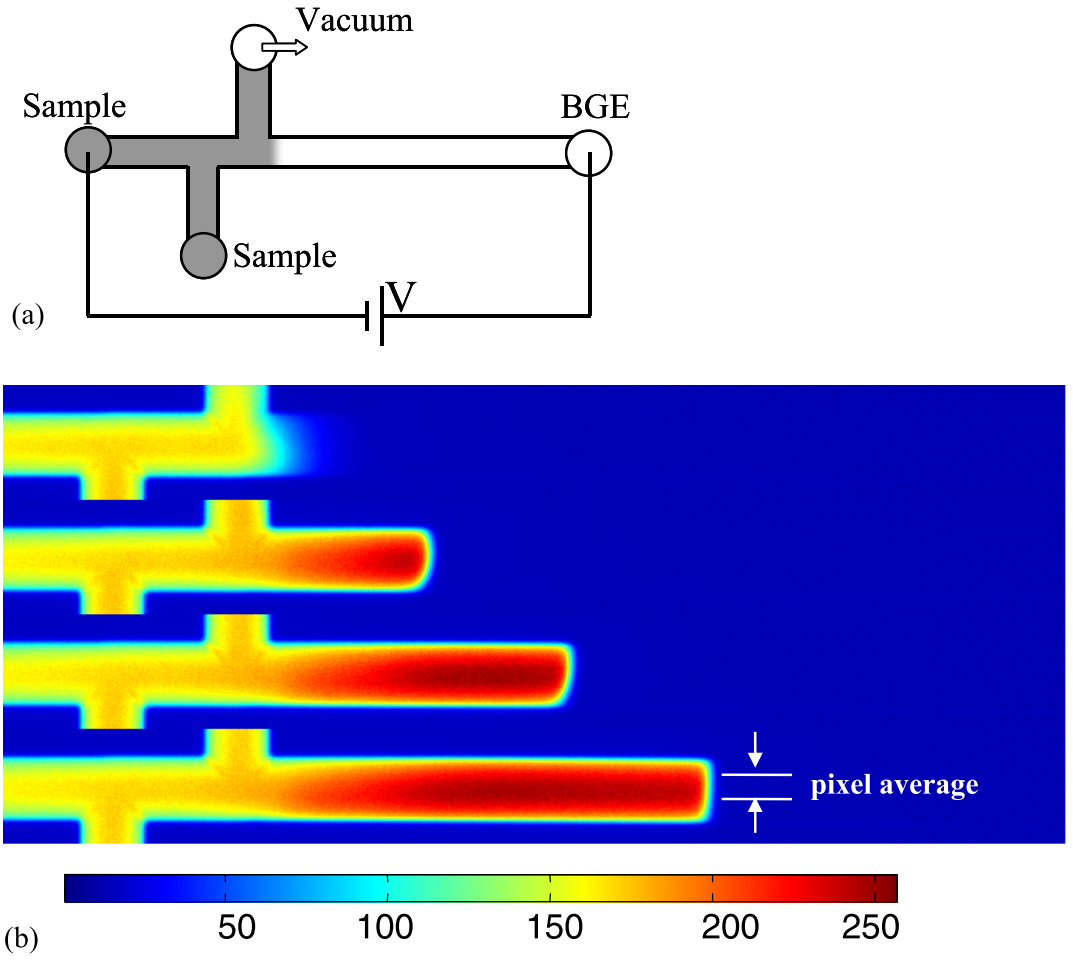

Figure 4. *(a) Schematic of microchip system used for the experiments. A vacuum is applied to generate the initial conductivity gradient. Once the gradient is established, an electric field is applied from right-to-left to initiate stacking of negatively charged sample ions. (b) CCD Images showing development of sample ion concentration distribution. In this case* $\gamma = 5$, $\beta = 0.25$, *and* $\varepsilon = 1$. *At these conditions, the sample ion distribution tends toward a shock wave in concentration at the leading edge of the sample region. The time between each frame was 132 ms, and the applied nominal electric field was 176 V/cm.*

the intensity data for the pixel regions of the microchannel images were averaged along the width of the channels, as indicated in Figure 4b, to form one-dimensional axial intensity profiles. Figures 5a shows the temporal development of the sample ion concentration distribution for $\gamma = 5$ under the $\beta < 1$ regime. The sample ion concentration increases to a maximum value of 1.3, much lower than γ. The axial width of the stacked region then continues to grow without further increase in peak concentration value, as predicted by the model. This regime is described in Figure 2b. The temporal and spatial development of concentration field for $\beta > 1$ regime is shown in Figure 5b. As predicted by theory, the concentration enhancement is greater than γ. Also, the rarefaction concentration wave is observed. This regime is described in Figure 2c.

Figure 5 also shows an overlay comparison between model predictions and experimentally measured concentration profiles for $\gamma = 5$. The model assumes constant current density whereas constant voltages are applied in the experiments. However, over the short time of the experiment, the current density is approximately constant. For a meaningful comparison, we fix the current density of the model such

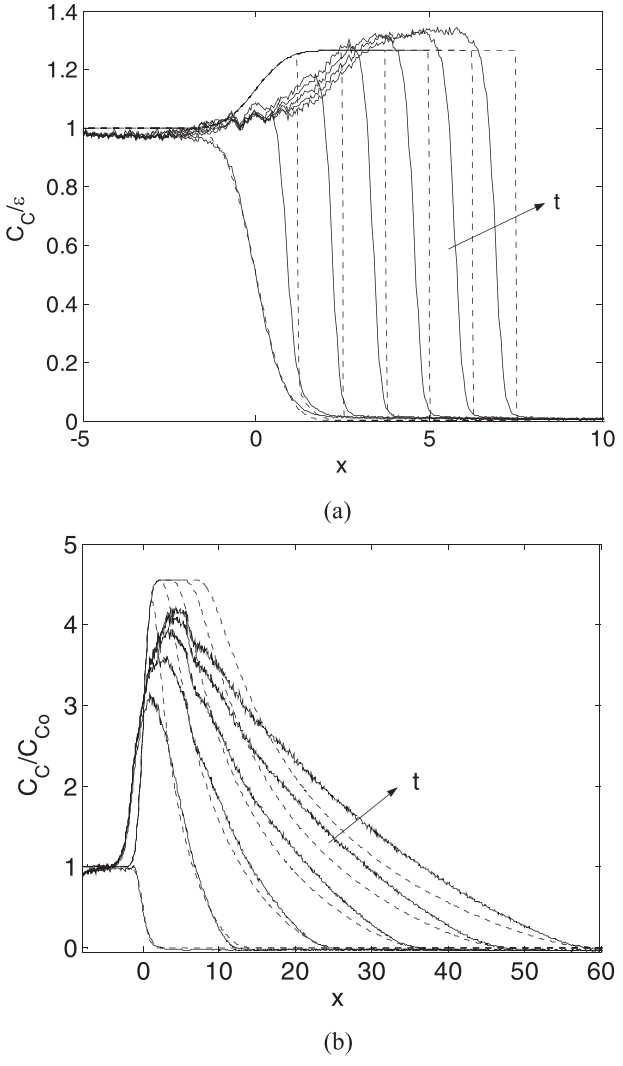

Figure 5. *(a) Comparison of measured and predicted sample ion concentration profiles for* $\gamma = 5$, $\varepsilon = 1$ *and* $\beta = 0.25$. *(b) Comparison of measured and predicted sample ion concentration profiles for* $\gamma = 1.9$, $\varepsilon = 0.5$ *and* $\beta = 2.3$. *Model predictions are shown as dotted lines. The time between each curve is 33 ms.*

that the initial electric field in the low conductivity sample, E_S, is equal to the expected value in the experiments. Since the length of the interface region is small compared to the length of the channel, E_S can be related to the applied potential as $E_S = \gamma V/L_T(1 + (\gamma - 1)a)$. Here, V is the applied voltage, L_T is the channel length and, a is the fraction of the channel occupied by the low conductivity sample. Figure 5 shows that there is good qualitative comparison in terms of the peak shapes and the temporal growth of the maximum concentration. The model neglects diffusion and convective effects, whereas in the experiments these effects lead to a slight broadening of sample profiles. The simple electromigrational model therefore underpredicts the time required to achieve the final concentration enhancement. However, as shown in Figure 6, the final value of maximum concentration enhancement is in very good agreement with the experiments. The error bars represent 95% confidence interval over five realizations for the three cases. These detailed comparison of the predicted and measured dynamics show that the electromigrational model can be used to quantitatively predict maximum concentration

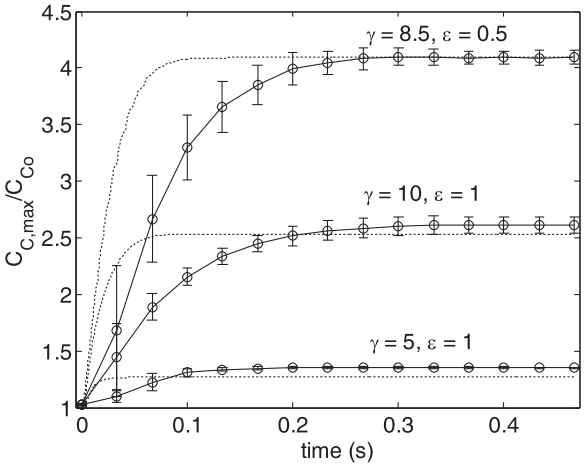

Figure 6. *Normalized sample ion peak concentration versus dimensional time for three values of γ and two values of ε. In all cases $\beta = 0.25$. The dotted lines are the model predictions and the circles are experimental results. The model accurately predicts the final value of concentration enhancement. However, since diffusion and other dispersive effects are neglected, the model under predicts the time taken to achieve the final concentration enhancement.*

enhancement and approximately predict the time required for this and the shape of concentration profiles. The model should be useful in optimizing FASS experiments with finite ε values.

7. Conclusions and Recommendations

We have developed an electromigration model to investigate the coupled, nonlinear dynamics of three fully ionized species across single electrolyte-electrolyte interface. We solved the resulting nonlinear hyperbolic equation using finite volume methods and conducted a parametric study. The degree of sample overloading is determined by ε. The ratio of the initial sample concentration to that of the initial counter-ion concentration in the sample region. For negligible values of ε, the maximum concentration enhancement approaches γ. For finite ε, model predictions show two distinct regimes of concentration enhancement. Transition between the two regimes is governed by β, the dimensionless ratio of the product of electrophoretic mobility and valence number of the sample ion and the co-ion. The regimes are as follows:

- For $\beta > 1$, the sample ion concentration field in the single electrolyte-electrolyte case is characterized by a rarefaction wave and maximum concentration enhancement is greater than γ. For a finite sample plug, a tailing peak is observed with maximum concentration enhancement values that may or may not be larger than γ (depending on, for example, the sample plug length).
- For $\beta < 1$, the sample ion concentration wave in the single electrolyte-electrolyte case develops sharp gradients and tends toward a concentration shock wave. For a finite sample plug, a fronting peak is predicted. For $\beta < 1$ cases, the maximum concentration enhancement is always less than γ.

We have experimentally validated the model for the two regime by using scalar epi-fluorescence imaging to measure the sample ion concentration fields. There is good qualitative comparison between the model predictions of the sample ion concentration profiles. There is good quantitative comparison between predicted and measured absolute values of maximum concentration enhancement.

Improved understanding of FASS process would be further aided by development of multi-species, electromigration-diffusion-convection models, which include equilibrium reactions and can handle the finite ε regime. Such tools would help to optimize FASS systems involving very low conductivity buffers or DI water as the sample matrix.

Acknowledgements. We gratefully acknowledge the advice of John Smith who commented on a version of this manuscript.

Funding Statement. J.G.S gratefully acknowledges funding by an NSF CAREER Award (Contract number NSF CTS0239080) with Dr. Michael W. Plesniak as contract monitor.

Declaration of Interests. The authors declare no conflict of interest.

Author Contributions. R.B. and J.G.S. created the research plan, designed experiments, and formulated analytical problem. R.B. led model solution and performed all experiments. R.B. and J.G.S. wrote the manuscript.

Data Availability Statement. Raw data are available from the corresponding author (J.G.S.).

Ethical Standards. The research meets all ethical guidelines, including adherence to the legal requirements of the study country.

Supplementary Material. Methods section and Supplementary information are available at https://doi.org/10.1017/flo.2021.1.

References

Bharadwaj, R., & Santiago, J. G. (2005). Dynamics of field-amplified sample stacking. *Journal of Fluid Mechanics*, *543*(57), 57–92.

Bharadwaj, R., Santiago, J. G., & Mohammadi, B. (2002). Design and optimization of on-chip capillary electrophoresis. *Electrophoresis*, *23*(16), 2729–2744.

Bier, M., Palusinski, O. A., Mosher, R. A., & Saville, D. A. (1983). Electrophoresis: Mathematical modeling and computer simulation. *Science*, *219*(4590), 1281–1287.

Burgi, D. S., & Chien, R. L. (1991). Optimization in sample stacking for high-performance capillary electrophoresis. *Analytical Chemistry*, *63*(18), 2042–2047.

Chien, R. L., & Burgi, D. S. (1991). Field amplified sample injection in high-performance capillary electrophoresis. *Journal Chromatography A*, *559*(1–2), 141–152.

Chien, R. L., & Burgi, D. S. (1992). On-column sample concentration using field amplification in CZE. *Analytical Chemistry*, *64*(8), 1046–1050.

Ermakov, S. V., Zhukov, M. Y., Capelli, L., & Righetti, P. G. (1994). Experimental and theoretical study of artifactual peak splitting in capillary electrophoresis. *Analytical Chemistry*, *66*(22), 4034–4042.

Foret, F., & Bocek, P. (1993). *Capillary zone electrophoresis.* New York, NY: VCH.

Gas, B., & Kenndler, E. (2000). Dispersive phenomena in electromigration separation methods. *Electrophoresis*, *21*(18), 3888–3897.

Gebaur, P., & Bocek, P. (1997). Predicting peak symmetry in capillary zone electrophoresis: The concept of the peak shape diagram. *Analytical Chemistry*, *69*(8), 1557–1563.

Hruska, V., Jaros, M., & Gas, B. (2006). Simul 5-free dynamic simulator of electrophoresis. *Electrophoresis*, *27*(5–6), 984–991.

Jacobson, S. C., & Ramsey, J. M. (1995). Microchip electrophoresis with sample stacking. *Electrophoresis*, *16*(1), 481–486.

Jung, B., Bharadwaj, R., & Santiago, J. G. (2003). Thousand fold signal increase using field-amplified sample stacking for on-chip electrophoresis. *Electrophoresis*, *24*(19–20), 3476–3483.

Jung, B., Bharadwaj, R., & Santiago, J. G. (2006). On-chip millionfold sample stacking using transient isotachophoresis. *Analytical Chemistry*, *78*(7), 2319–2327.

Kohlrausch, F. (1897). About concentration shifts due to electrolysis in the interior of solutions and mixed solutions. *Annalen der Physik*, *298*(10), 209–239.

Kuban, P., Berg, M., Garcia, C., & Karlberg, B. (2001). On-line flow sample stacking in a flow injection analysis–capillary electrophoresis system: 2000-fold enhancement of detection sensitivity for priority phenol pollutants. *Journal of Chromatography A*, *912*(1), 163–170.

Leveque, R. J. (2002). *Finite volume methods for hyperbolic equations.* Cambridge: Cambridge University Press.

Liu, Y, Foote, R. S., Jacobson, S. C., & Ramsey, J. M. (2005). Stacking due to ionic transport number mismatch during sample sweeping on microchips. *Lab on a Chip*, *5*, 457–465.

Mosher, R. A., Saville, D. A., & Thormann, W. (1992). *Dynamics of electrophoresis*. New York, NY: VCH.

Preisler, J., & Yeung, E. S. (1996). Characterization of nonbonded poly (ethylene oxide) coating for capillary electrophoresis via continuous monitoring of electroosmotic flow. *Analytical Chemistry*, *68*(17), 2885–2889.

Whitham, G. B. (1974). *Linear and nonlinear waves.* New York, NY: Wiley-Interscience.

Cite this article: Bharadwaj, R., & Santiago, J. G. (2021). Shockwave and rarefaction phenomena in field amplified sample stacking of sample ions. *Flow*, *1*, E1. doi:10.1017/flo.2021.1